

Recombination processes in *a*-Si:H. A study by optically detected magnetic resonance

F. Boulitrop*

Groupe de Composants Electroniques du Laboratoire d'Electronique et de Technologie de l'Informatique (LETI/CE) et Section de Résonance Magnétique du Département de Recherche Fondamentale (DRF/RM), Centre d'Etudes Nucléaires de Grenoble, F-38041 Grenoble Cedex, France

(Received 30 June 1983)

We report cw and time-resolved optically detected magnetic resonance data on samples of *a*-Si:H prepared by reactive sputtering, glow-discharge, and chemical vapor deposition. Two distinct luminescence processes are inferred near 1.3–1.4 and 0.9 eV. An enhancing signal at $g=2.0065$ is observed on the 0.9-eV photoluminescence (PL) band and is linked to distant-pair radiative recombination between a dangling bond and a hole localized in a valence-band tail state. The high-energy PL band shows a quenching resonance at $g=2.005$, which can be associated with shunt processes involving dangling bonds. Enhancing signals are also observed on this high-energy band: In low-defect-density sputtered samples, a 200-G-wide line at $g \approx 2.01$ is associated with short radiative lifetimes (\sim ms) and narrows for longer lifetimes (\sim s). In all other samples studied, a narrower line (19 G) at $g=2.0078$ is linked to short lifetimes and broadens for longer lifetimes. Both signals are consistent with a model in which the high-energy PL band arises from radiative recombination of carriers localized in band tail states, and are successfully explained by exchange interaction.

I. INTRODUCTION

The photoluminescence (PL) of *a*-Si:H, first observed by Engemann and Fischer,¹ consists at low temperature of a broad featureless band peaking between 1.25 and 1.4 eV in low-spin-density intrinsic samples. Higher spin density, doping, and measurement temperatures above 200 K quench this band and enhance another band peaking around 0.9 eV, associated with defects such as dangling bonds. The high-energy band is usually attributed to radiative recombination between carriers localized in band tail states² and has been extensively studied. Nevertheless there is little agreement on the details of the recombination processes. It is not yet agreed whether its kinetics are geminate or distant pair,^{3,18} nor whether it is significantly Stokes shifted or is due to essentially zero-phonon transitions.^{5,6}

However, we have suggested a model in which photoexcited carriers thermalize down the bands and the band tail states and localize in local minima in energy of the band tail states⁷; in this model, the high-energy PL band arises from radiative distant-pair recombination of these localized carriers. This model is supported by a simulation of the PL spectrum by convolution of the energy distributions of the conduction- and valence-band tail states' minima, and by good fits of the excitation energy and temperature dependences of the PL spectrum.⁷

In intrinsic samples, electron spin resonance (ESR) detects a single signal at $g=2.0055$ attributed to dangling bonds,⁸ while light-induced ESR (LESR) selects two resonances at $g=2.004$ and $g=2.012$ thought to be associated with conduction- and valence-band tail states, respectively.^{9,10} The PL quantum efficiency has been linked to the dangling-bond density in that a spin density of greater than 10^{17} cm^{-3} results in a strong quenching of the photoluminescence.¹¹ The evolution of the mean PL decay time

and the LESR spin density with temperature have been found to be very similar.¹² However, no direct experimental evidence associates the PL processes with ESR or LESR centers.

Optically-detected magnetic resonance (ODMR) measures changes in luminescence intensity when static magnetic field and microwave power are applied to the sample at the recombination centers' resonance conditions. Thus, this technique helps deconvolve unresolved components of a broad luminescence band and associate luminescence bands with ESR centers.¹³ Previous ODMR studies in *a*-Si:H identified up to five different resonances, two resulting in a negative effect (quenching signals), and three others in increases (enhancing signals) of the PL intensity.^{14,15} These resonances are superimposed around $g=2$. These similar values of the g factor and the relatively large linewidths (> 10 G) make deconvolutions often tentative. Selection of the PL energy is not enough to isolate the different resonances in order to perform the correct g factor and linewidth measurements necessary for the comparison of these signals with the ESR resonances. These overlaps between signals have led to different interpretations of the ODMR results. LESR centers have been considered as either radiative¹⁵ or nonradiative¹⁶ and it has been suggested that dangling bonds rather than band tails are the radiative centers giving rise to the main luminescence band.¹⁷

This luminescence band possesses a very large distribution of decay time extending from nanoseconds to seconds.^{3,18} Time-resolved ODMR (TRODMR) has recently been used successfully to study donor-acceptor recombination in crystalline semiconductors where lifetime distributions are also often very broad.¹⁹ In *a*-Si:H, TRODMR results have already been reported¹⁵ but we think that interpretation of these data is difficult as discussed in the next section. A promising preliminary re-

port of a frequency-resolved ODMR study has been published²⁰ but this technique seems at the present time, to be limited by a poor signal-to-noise ratio. In the TRODMR study reported here, we have used a pulsed microwave technique which improves signal-to-noise ratio, minimizes interferences between signals, and yields reliable time-resolved data.

In this paper we report studies of ODMR and TRODMR in samples made by the three major techniques: reactive sputtering (SP), glow discharge (GD), and chemical vapor deposition (CVD). In Sec. II the different experimental setups are described and different cw ODMR and TRODMR techniques are discussed. Section III describes the ODMR and TRODMR data including spectral and temperature dependences. Deconvolutions of several ODMR signals into ESR and LESR resonances are reported. We also describe some time-resolved optically-detected electron nuclear double resonance results. We finally discuss in Sec. IV different recombination processes in *a*-Si:H, interactions between recombining carriers and their interaction with their nuclear environment. We will then suggest an improvement of our recombination model outlined above in which the centers and the recombination processes involved in each signal are identified.

II. EXPERIMENTAL DETAILS

A. Experimental techniques

As required by the optical selection rules, the rate at which a pair of photoexcited carriers recombines depends on its spin configuration. Thus, if under optical excitation, carriers are created with an isotropic spin distribution, the population of the slow-decaying pairs becomes rapidly larger than the population of the fast-decaying pairs and a spin correlation appears. Application of microwave power at resonance will restore an isotropic spin distribution, will increase the population of the fast-decaying pairs, and thus will enhance the luminescence intensity.²¹

Continuous-wave (cw) ODMR measures variations of the luminescence intensity under continuous optical excitation and square-wave modulation of the microwave power. TRODMR observes changes induced by the microwaves in the luminescence decay which follows an optical excitation pulse. These changes in the decay are measured by gating the output of the detector at a given delay time after the excitation pulse, then subtracting the gated output corresponding to the decay without microwaves from the one with microwaves, with the use of a boxcar analyzer or a lock-in amplifier. This sequence (excitation plus decay with microwaves and excitation plus decay without microwaves) is repeated in order to improve the signal-to-noise ratio of the experiment. The shorter the delay time, the narrower is the gate and the larger must be the repetition rate in order to keep the overall measurement time constant. Interpretation of the TRODMR results in *a*-Si:H for delays shorter than a few hundred μ s is rather difficult because of the accumulation

of carriers decaying on a longer time-scale than the repetition rate.¹⁸ These accumulated carriers react to the microwaves and interfere with the real TRODMR signal.²⁰ TRODMR effects for delay times longer than a few hundred μ s are measured for repetition rates less than 1 kHz, rates at which the accumulated carrier density is negligible for the high-excitation density used.

Microwave power is applied either during the whole decay or during a short pulse in phase with the gate of the detector. The first technique has been recently used by the Xerox group in *a*-Si:H (Ref. 15) and we report in this paper a TRODMR study for which we used the second technique. This second technique has also been used by Morigaki *et al.*³⁶

When microwave power is applied during the whole decay, the spin populations are always equal as the slow pairs can decay through a spin flip. A positive TRODMR effect is measured for delays around the radiative decay time of the fast pairs (R_f^{-1}) and a negative TRODMR effect is measured for delays around the radiative decay time of the slow pairs (R_s^{-1}) as shown in Fig. 1(b). Since radiative distant pairs may give positive and negative TRODMR signals, interpretation of the results is thus more difficult than for cw ODMR.

On the other hand, if no microwave power is applied during the first part of the decay, the population of the slow-decaying pairs will be much larger than the popula-

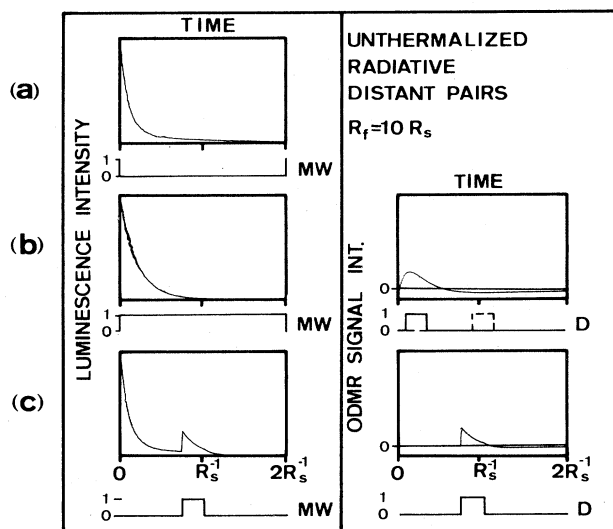


FIG. 1. Comparison between the two TRODMR techniques. A simple, unthermalized, radiative distant-pair system is considered. The lifetime of a pair in the slow-decaying spin configuration (R_s^{-1}) is assumed to be 10 times the lifetime of a pair in the fast-decaying spin configuration (R_f^{-1}). The luminescence decays emitted by this system after an excitation pulse are shown on the left: (a) without microwave power; (b) with microwave power applied during the whole decay; (c) with a microwave pulse applied sometime during the decay. The TRODMR effect is the difference between the decay without microwaves and the decay under resonant microwave irradiation and is shown for both techniques [(b)-(a) and (c)-(a)] on the left-hand side.

tion of the fast-decaying pairs. Application to the sample of a microwave pulse at resonance will equalize both pair populations and will produce a transient positive spike on the luminescence decay [Fig. 1(c)]. Since the gate on the output of the detector is set on this spike, radiative distant pairs yield only positive TRODMR signals. The main source of noise in ODMR experiments comes from fluctuations on the luminescence intensity caused by fluctuations of the laser intensity or by mechanical vibrations. Since this pulsed microwave technique measures a large relative effect [Fig. 1(c)], the signal-to-noise ratio is larger than for the other TRODMR method and for cw ODMR. This large transient spike dominates any negative effect resulting from spin-dependent shunt mechanisms: If the gate on the output of the detector and the microwave pulse are simultaneous and short compared to the decay time associated with the shunt process in its fast spin configuration, the enhancing TRODMR signal will be much larger than the TRODMR quenching signal associated with shunt mechanisms.²² When these quenching signals are studied the microwave pulse is set before the gate on the output of the detector. Interferences between signals of opposite sign are thus minimized. For a more detailed study of the enhancing signals, it is sometimes useful to measure the effect on the signal of a shift between the microwave pulse and the detection gate. Pairs are then selected as a function of separation according to their fast radiative decay time rather than by their slow-decay time. However, no effect on the line shape is observed in our case. This might be an indication that these two decay times are similar within an order of magnitude.

B. Experimental setup

ODMR experiments were carried out in a modified Varian model-4500 X-band ESR spectrometer equipped with an Oxford EPR 900 continuous helium gas-flow cryostat. The temperature range accessible is 3.7 K to room temperature. The sample is optically excited by 5145-Å radiation from an argon laser. Luminescence is detected either by cooled germanium detectors with different response times (100 ns, 300 μ s), limited to radiation of energy above 0.75 eV, or by a lead sulfide detector for far-infrared luminescence. Passband filters or a HR 20 Jobin Yvon spectrometer are inserted between sample and detector. Microwaves are chopped by a *p-i-n* diode attenuator (on, 2 dB; off, 80 dB) and amplified when necessary by a traveling-wave tube (TWT), giving up to 10 W available at the cavity. Changes in the photoluminescence intensity induced by the microwaves are detected by a lock-in amplifier. The magnetic field is slowly scanned through the resonance, its value being continuously measured by a self-tracking NMR Gaussmeter. This value and the lock-in output, i.e., the size of the ODMR signal are digitally stored into a computer. This technique proved to be of great help for precise *g* value and linewidth measurements when signal-to-noise ratio is poor. A 3-kHz sine-wave-modulated magnetic field can be superimposed on the static field in order to enhance broad lines.²³ The size of this modulated field can be set from 0 to 20 G. The spec-

tral dependence of an ODMR signal, i.e., $\Delta I(\lambda)$ is measured by setting the field on the resonance and by scanning the PL spectrum with a spectrometer. The PL spectra and the spectral dependences are corrected for the detection system response. The shape of the time response of the PL intensity to a microwave power modulation is observed using a digital multichannel analyzer which improves signal-to-noise ratio by successive accumulation of the response.

During pulsed microwave time-resolved experiments, the laser excitation is pulsed by an acousto-optic modulator (extinction ratio: 1/500). Sometime during each second luminescence decay, a microwave pulse is applied to the cavity containing the sample. Changes thereby induced in the decay are measured by gating the detector's output at a given delay time after the excitation pulse and by subtracting the decay without microwaves from the decay with microwaves, using a lock-in amplifier. The different pulses required (excitation, microwaves, detector, and lock-in reference) are supplied by a programmable pulse generator interfaced to the computer. Once a suitable pulse sequence is found, delay times are modified by changing the repetition rate. Typical pulse sequences are shown in the insets of Figs. 8 and 13.

Time-resolved optically-detected electron nuclear double resonance (TRODENDOR) experiments are performed using a sample holder with a copper loop in the vertical plane parallel to the magnetic field. Radiofrequency (rf) power is applied to this loop. The magnetic field is set at a given point of the TRODMR line and frequency of the rf power is scanned. Changes in the TRODMR intensity are recorded. No ENDOR effects could be measured on the cw ODMR signals.

C. Samples

For this study we used samples made by the three major preparation techniques: reactive sputtering, glow-discharge of silane, and chemical vapor deposition from silane. For each kind of sample, the hydrogen concentration has been measured by nuclear reaction with Boron 11 and defect densities were calculated from the intensity of the ESR signal at $g=2.0055$. All samples, about 1 μ m thick, were deposited on Spectrosil quartz.

Samples of *a*-Si-H made by reactive sputtering were prepared from a 70% H₂-30% Ar mixture and using 250 W of radiofrequency power, onto a substrate held at 250°C. Their ESR densities in the dark are around 5.10¹⁵ cm⁻³. These samples contain an average of 30% atomic hydrogen. Some deuterated amorphous silicon samples were prepared by this technique, hydrogen being replaced by deuterium in the argon mixture.

One of the sputtered *a*-Si:H samples was annealed for one hour at 490°C under argon flow, in order to decrease its hydrogen concentration to 5%. Its ESR spin density increased then to 3 \times 10¹⁷ cm⁻³.

CVD samples were prepared at 600°C by chemical vapor deposition from silane. They were posthydrogenated at 400°C in a hydrogen plasma, and contain about 3%

hydrogen. Their dark ESR spin density is around 10^{17} cm^{-3} .

GD samples were made by glow-discharge decomposition of pure silane onto substrates held at 250°C . Their hydrogen concentration is around 8% and their dark ESR spin density around 10^{16} cm^{-3} .

III. EXPERIMENTAL RESULTS AND IDENTIFICATION OF SIGNALS

In Fig. 2, we show the four kinds of signals that we see by cw ODMR in *a*-Si:H. We have a narrow quenching signal at $g=2.005$, a broad enhancing line around $g=2.01$, and a narrow enhancing signal at " $g=2.0085$." The latter could not be observed in our low-defect-density sputtered samples and its g factor is quoted because this line could not be completely isolated from the quenching signal during cw ODMR measurements in any of the other samples as seen later by TRODMR. These three lines are ODMR effects on the main luminescence band. A last narrow ODMR enhancing signal at $g=2.0065$ is associated with the 0.9 eV defect-related luminescence band. In this section we will describe the different experimental results associated with these signals.

A. The quenching signal at $g=2.005$

This signal, observed in all samples studied, corresponds to a decrease of the luminescence intensity. The relative

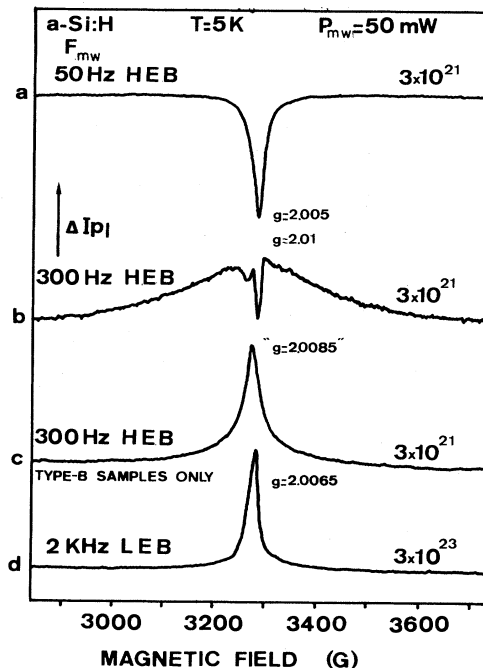


FIG. 2. cw ODMR spectra in *a*-Si:H. The microwave chopping frequency F_{MW} , the selected luminescence energy (HEB indicates the 1.4-eV band; LEB, the 0.9-eV band, where HEB denotes high-energy band and LEB denotes low-energy band) and the excitation rate (pairs $\text{cm}^{-3} \text{ s}^{-1}$) are indicated for each spectrum. Signals *a*, *b*, and *d* are observed in all samples while signal *c* cannot be measured in low-defect-density sputtered *a*-Si:H. All spectra were measured at $T=5 \text{ K}$, 50 mW microwave power.

size of the effect ($\Delta I/I$) is larger at low-optical-excitation density. This line is asymmetric, its maximum is for $g=2.005$ and its linewidth is 13 G. These characteristics are independent of sample preparation and measurement temperature. Other authors report two different quenching signals.¹⁵ We only found one and we might possibly suggest, in agreement with the Hull group,¹⁶ that the signal these authors called Q_2 is the result of an interference between the quenching signal at $g=2.005$ and the narrow enhancing signal at $g=2.0085$.

The spectral characteristics of this quenching line are very sensitive to microwave power: At high power it becomes symmetric, broadens, and shifts toward low fields. This asymmetry and behavior with increasing microwave power strongly suggest that this line is the sum of at least two indissociable resonances. It has been compared by other authors to the LESR signal.²⁴ The agreement being fairly good, it has been concluded that these two signals are identical. However, in intrinsic *a*-Si:H samples, the g factor of the LESR signal equals 2.0045. In *X* band this g factor difference corresponds to 1 G and is significant although the linewidths are large. Now if we try to simulate a line with $g=2.005$ by a sum of the two components of the LESR signal at $g=2.004$ and $g=2.012$ we get linewidths ($\sim 20 \text{ G}$) much larger than that measured (13 G). It is necessary to sum the two LESR resonances and the dangling-bond signal at $g=2.0055$ in order to fit this ODMR quenching signal [Fig. 3(a)]. Dangling bonds as well as LESR centers seem involved in the quenching signal.

In Fig. 4, we compare the spectral dependence—i.e., $\Delta I(\lambda)$ —of this quenching signal with the photoluminescence spectra in different samples. In the low-spin-density sputtered samples as we will see in the following paragraphs, no narrow enhancing signal is observed. Thus, there is no interference with the quenching signal. We notice that the spectral dependence and the luminescence spectrum are similar. The two maxima are only 40 meV

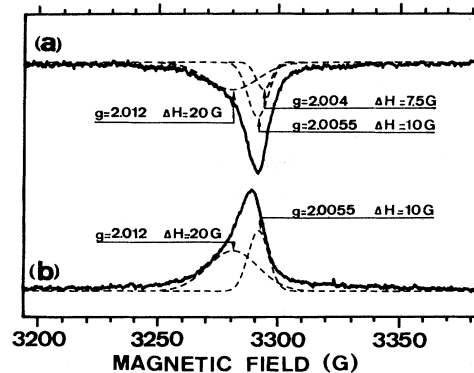


FIG. 3. (a) Fit of the quenching line by linear combination of the components at $g=2.012$ and $g=2.004$ of the LESR signal and the ESR resonance at $g=2.0055$ associated with dangling bonds. (b) Fit of the enhancing line at $g=2.0065$ by linear combination of the component at $g=2.012$ of the LESR signal and the ESR resonance at $g=2.0055$.

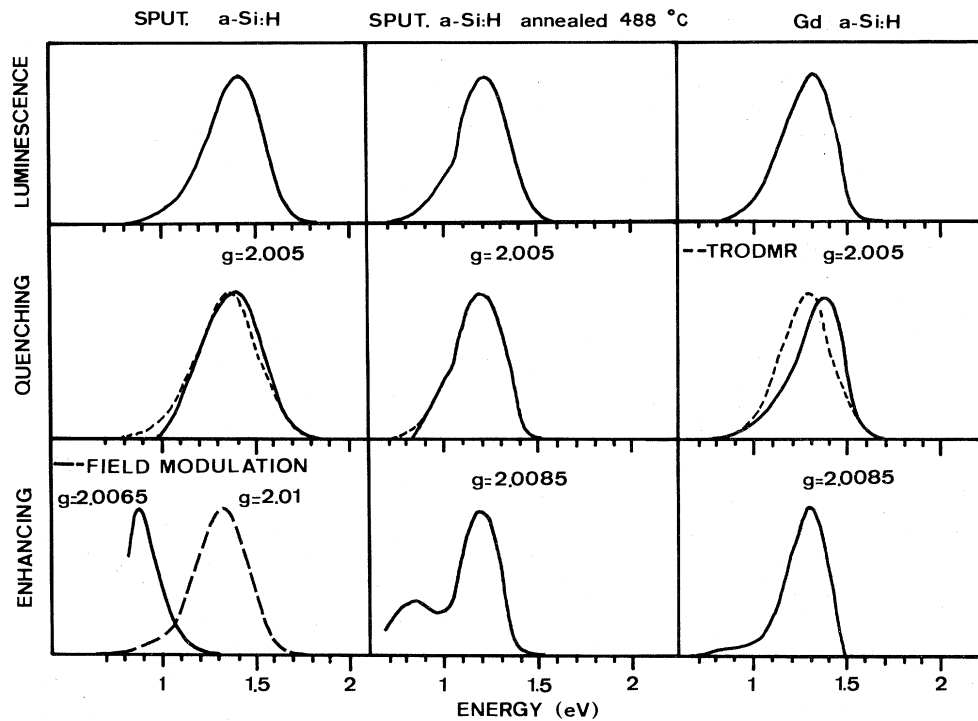


FIG. 4. Luminescence spectra and cw ODMR spectral dependences of the quenching and enhancing signals in three types of samples. TRODMR spectral dependences of the quenching signal (broken curves) are, however, the correct spectral dependences of the quenching signal (see text). Field modulation was necessary to measure the spectral dependence of the 200-G-wide enhancing line around 2.01 (broken curve).

apart. In contrast, in glow-discharge, CVD, and annealed sputtered samples the cw spectral dependence of the quenching signal is shifted toward high energies compared to the luminescence spectra (Fig. 4). We suggest that this difference between the two spectra is a result of the interference of the narrow enhancing signal at $g=2.0085$, always present in these samples, with the quenching signal. This suggestion is confirmed by the spectral dependences of the quenching signal as measured by time-resolved ODMR (Fig. 4). Since our pulsed microwave TRODMR technique is much more efficient than cw ODMR for separating the two signals, we find that even in these samples the spectral dependence of the quenching signal is identical to the luminescence spectra.

The first reports of ODMR studies^{4,24} showed the influence of the microwave chopping frequency and of the lock-in phase setting on the ODMR signals. These effects were explained later by the shape of the response of the luminescence intensity to the microwaves.¹⁶ In Fig. 5(a) we show a typical response of the quenching signal to square-wave-chopped microwaves. A simple exponential evolution toward equilibrium is observed at the application and at the removal of the microwaves. No transient spike is observed. Time constants associated with the decay and the rise vary with excitation density and temperature and are in the millisecond range.

When the measurement temperature is increased, the intensity of the ODMR signal decreases (Fig. 6). From 5 to

80 K the signal is reduced by a factor of 4 while the luminescence intensity is constant. The quenching signal becomes undetectable above 150 K in the samples studied. Neither shift, nor change in shape or width of this line has been seen during TRODMR experiments over the whole

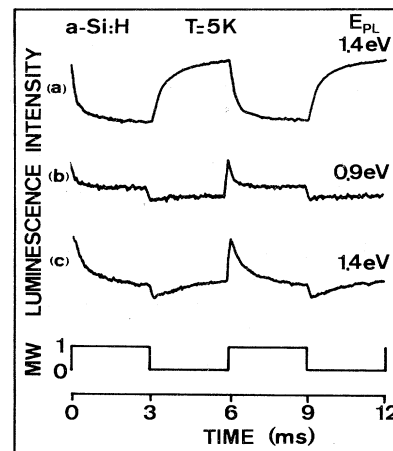


FIG. 5. Response of the luminescence intensity to a square-wave modulation of the microwave power. (a) Quenching signal at $g=2.005$, (b) enhancing signal at $g=2.0065$, (c) enhancing signal on the high-energy band. Pair-creation rates are (a) $2.10^{21} \text{ cm}^{-3} \text{ s}^{-1}$, (b) $2.10^{22} \text{ cm}^{-3} \text{ s}^{-1}$, and (c) $2.10^{20} \text{ cm}^{-3} \text{ s}^{-1}$.

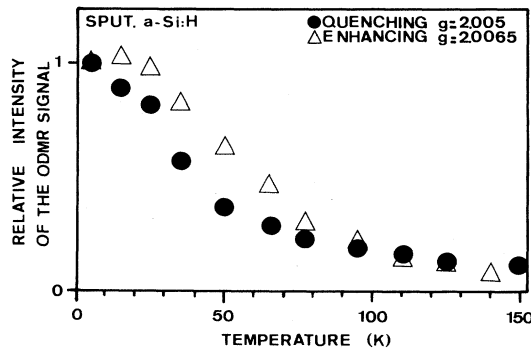


FIG. 6. Temperature dependence of the quenching cw ODMR signal at $g=2.005$ and of the enhancing cw ODMR signal on the low-energy band at $g=2.0065$.

available delay-time range (100 μ s, 300 ms). No ODENDOR nor TRODENDOR signal could be detected on this quenching line.

B. The enhancing signal at $g=2.0065$ on the low-energy band

This signal is stronger in the low-defect-density sputtered samples than in the others. The relative size of the ODMR effect is larger at high excitation densities. This line is asymmetric, its maximum is at $g=2.0065$, and its linewidth is 15 G. These characteristics are independent of sample preparation and measurement temperature. This signal, too, is very sensitive to microwave power: At high power it becomes symmetric, broadens, and shifts toward low fields. This suggests that this line is the sum of at least two indissociable resonances. A good fit is obtained using the LESR hole-state resonance at $g=2.012$ and the dangling-bond resonance at $g=2.0055$ [Fig. 3(b)]. This deconvolution is in agreement with other authors.¹⁷

In Fig. 4, the spectral dependences of this enhancing signal in different samples are shown. Because of the absence of the narrow, enhancing signal at $g=2.0085$ in low-defect-density sputtered samples, the spectral dependence of the line at 2.0065 is well isolated for such samples. It is roughly a 200-meV-wide Gaussian profile centered around 0.85 eV. Since the germanium detector used for these measurements is blind to light of wavelength larger than 1.6 μ m (0.75 eV), we used a cooled PbS detector and a high-pass germanium filter to study very-low-energy luminescence in *a*-Si:H. The luminescence spectrum extends down to 0.45 eV.²⁵ We have measured the ODMR signal on this low-energy part of the luminescence spectrum and found the same enhancing line at $g=2.0065$ (Fig. 7). We conclude that this low-energy part of the PL spectrum is not due to a third luminescence band but is only the low-energy tail of the 0.85-eV band.

In Fig. 5(b), we show a typical response to square-wave-chopped microwaves for the 2.0065 enhancing line. The shape of this response is very sensitive to optical excitation density.^{16,25} We notice a strong positive transient

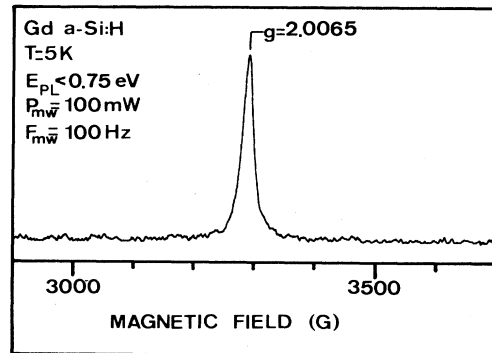


FIG. 7. cw ODMR spectrum associated with the low-energy part (<0.75 eV) of the PL spectrum. A crystalline germanium filter and a lead sulfide detector were used to select this luminescence.

spike when microwaves are applied and a negative spike when microwaves are removed. The difference between the equilibrium levels just before the application and the removal of the microwaves is much larger for high-optical-excitation densities.

Time-resolved experiments on this line yields lifetimes shorter than 100 μ s for carriers involved in the low-energy luminescence band (Fig. 10). Neither shift nor change in shape or width of this line has been seen over the whole delay time range available in our TRODMR experiments. This signal slowly decreases when temperature is increased above 20 K and is hardly detectable above 150 K (Fig. 6). No ODENDOR nor TRODENDOR signal could be detected on this enhancing line.

C. The enhancing signals at high energy

If we consider the results of ODMR or TRODMR on the enhancing signals on the high-energy band we have two kind of samples. First, we have the low-defect-density sputtered samples containing 30% hydrogen which we will call type *A*. Second, we have all the other samples (glow-discharge, CVD, and annealed sputtered) containing less than 10% hydrogen which we will refer to as type *B*.

1. Type-A samples

In sputtered samples, a 200-G-wide line at $g \approx 2.01$ is observed by cw ODMR when a 3-kHz sine-wave-modulated magnetic field is superimposed on the static field. This field-modulation technique is a classical method to enhance inhomogeneously broadened lines.²³ This line is symmetric and has a perfect Lorentzian line shape. The relative intensity of this signal is larger at low optical excitation power.

During time-resolved measurements, the 2.005 quenching and the 2.0065 enhancing signals' line shapes were independent of delay time. We notice in Fig. 8 that this is, however, not true as far as the enhancing signal on the main luminescence band is concerned. While for delay times less than 100 μ s no signal at all can be seen on the

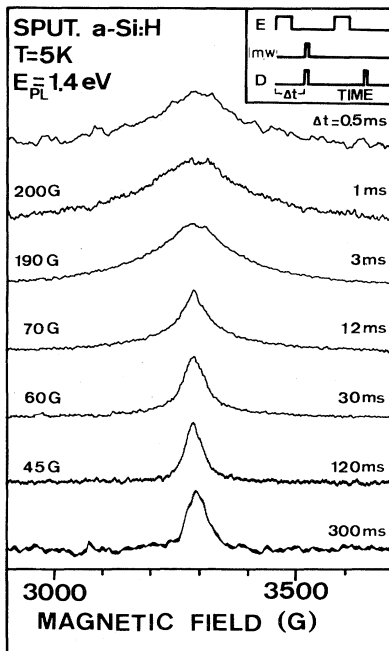


FIG. 8. Pulsed-microwave TRODMR spectra measured in *a*-Si:H samples prepared by reactive sputtering. Delays are varied from 0.5 to 300 ms by an increase of the repetition rate with the shape of the pulse sequence (shown in the inset) kept constant. Microwave power is also decreased from 2 W (0.5 ms) to 3 mW (300 ms) in order to keep the product of the width of the microwave pulse and the microwave power constant. The number of spin transitions induced by the microwaves during each pulse is thus kept constant if the matrix element is constant.

main luminescence band, a 200-G-wide line similar to the cw ODMR signal is measured when the delay time is increased to a few hundred μ s. This line reaches its maximum in intensity for delays of a few ms. The line shapes and width of this signal are independent of microwave power²⁵ in contradiction with other reports.¹⁵ At longer delay times, the signal narrows and becomes the sum of two lines of different width having similar *g* values. For delays of a few hundred ms, a single 45-G-wide Lorentzian line remains. A TRODMR effect is still measured for delay times as long as a few seconds.²⁵ These signals can be enhanced up to a factor of 10 by magnetic field modulation. None of these lines are similar to the ESR or LESR resonances. A weak negative TRODENDOR signal centered at the distant proton NMR resonance frequency (14 MHz) is measured for a 3-ms delay time (Fig. 9).

The spectral dependence of the cw ODMR signal is shown in Fig. 4. It is shifted by 70 meV toward low energy compared to the luminescence spectrum. This spectral dependence is confirmed when measured by TRODMR for delays of order ms (Fig. 10); however, it peaks only 50 meV lower in energy than the time-resolved luminescence

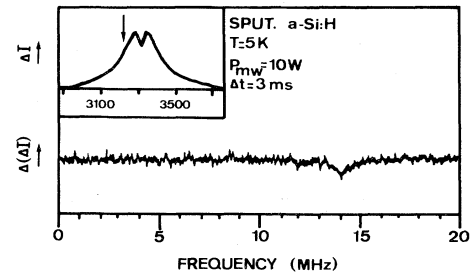


FIG. 9. TRODENDOR spectrum showing a quenching effect, i.e., a reduction of the ODMR signal at the distant proton nuclear resonance frequency. Magnetic field was set on the shoulder of the 200-G-wide TRODMR line, as shown by the arrow in the inset. A 5-G, 3-kHz sine-wave-modulated magnetic field was superimposed on the static field in order to increase signal-to-noise ratio.

spectrum measured at the same delay (Fig. 10).

The luminescence spectra of hydrogenated amorphous silicon and deuterated amorphous silicon prepared by reactive sputtering under the same conditions are very similar (Fig. 11). In Fig. 12 we show TRODMR spectra of this *a*-Si:D sample. We notice a difference with the results measured for *a*-Si:H. At a 3-ms delay the signal is the sum of the broad resonance and a narrow line. However, the width of the broad resonance is still 200 G.

In weakly *n*- or *p*-type sputtered samples ODMR and TRODMR are unchanged. When doping is increased and as soon as the low-energy, defect-related luminescence band dominates,²⁶ the enhancing signal at *g*=2.0065 becomes the only ODMR or TRODMR detectable effect.

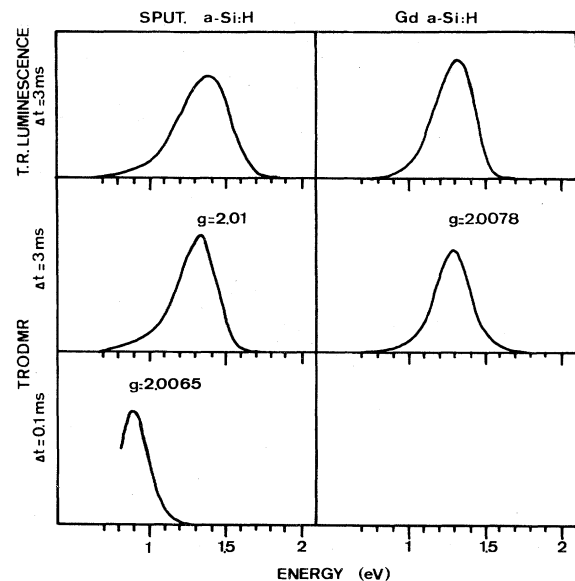


FIG. 10. Time-resolved luminescence spectra and TRODMR spectral dependences of the enhancing signals in two types of samples.

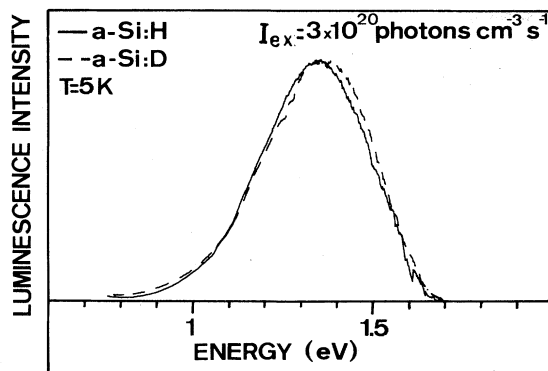


FIG. 11. Luminescence spectra of two samples of *a*-Si:H and of *a*-Si:D prepared by reactive sputtering under the same conditions.

2. Type-B samples

In all other samples, cw ODMR detects the broad enhancing line already reported in type-A samples and in addition a narrow enhancing line. This narrow line is asymmetric, 19 G wide, and its g factor is 2.0085. It has a much stronger effect ($\Delta I/I$) on the luminescence intensity than the broad line. However, we think that during cw ODMR measurements the quenching signal always interferes and so these resonance parameters are not correct.

During time-resolved experiments this narrow line is measured at short delays (few hundred μ s). When a proper pulse sequence is used to decrease the quenching signal intensity considerably, the narrow enhancing line then becomes symmetric, Lorentzian, and its g factor equals 2.0078. As delays are increased to the ms timescale, this line is superimposed on the 200-G broad line (Fig. 13). As delays are further increased, the TRODMR signal becomes similar to the one measured in type-A samples for the same delay time. In these samples too, ODMR effects are measured for delays as long as several seconds.²⁵ The spectral dependence of the narrow signal at $g=2.0078$ is similar to the luminescence spectrum as shown in Fig. 10.

The microwave transient response of this narrow enhancing signal is shown in Fig. 5(c). This response is

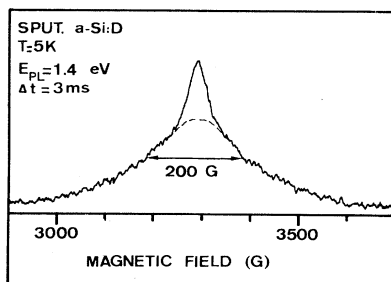


FIG. 12. TRODMR spectrum measured for a delay of 3 ms in a sample of *a*-Si:D prepared by reactive sputtering. Although this spectrum is a superposition of two lines, it is clear that the width of the broader line is ≈ 200 G.

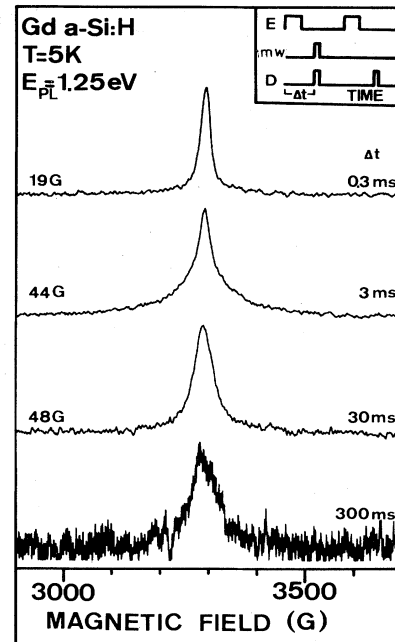


FIG. 13. Pulsed-microwave TRODMR spectra measured in *a*-Si:H samples prepared by glow discharge from silane. Delays are varied from 0.3 to 300 ms. Other details are the same as for Fig. 8.

similar to the one measured on the enhancing signal at $g=2.0065$ on the low-energy luminescence band. Under a wide range of conditions these transient measurements show the interference between the quenching signal and the narrow enhancing signal at $g=2.0078$.^{16,25} Under some conditions such as those used for the response of Fig. 5(c), this interference effect can be minimized.

D. Summary

The most important characteristics of the ODMR and TRODMR signals reported in the previous paragraphs of this section are summarized in Table I.

IV. DISCUSSION

The interpretation of the experimental results reported in the preceding section must consider the following two questions: What are the centers involved in each signal (tail states, dangling bonds, or other centers)? What kind of recombination process are these centers taking part in: nonradiative or radiative, and if radiative, at which energy? In this section, we will first review the experimental results and the different interpretations already reported in the literature by other groups. We will then try to answer these two questions for the enhancing signal at $g=2.0065$, the quenching signal at $g=2.005$, and the enhancing signals on the high-energy luminescence band. We will also discuss the origin of the 200-G linewidth of the latter in type-A samples.

TABLE I. Summary of the important characteristics of the ODMR and TRODMR signals.

Temperature (K)	Name	Sign	<i>g</i> factor	Width $H_{1/2}$ (G)	Samples	Spectral dependence (eV)	Excitation dependence	Deconvolution	Time resolved
5	Q	—	2.005	13	All	1.4–1.3	—	2.0055 2.012 2.0043	same
5	E_L	+	2.0065	15	All stronger in A	0.85	+	2.0055 2.012	same
5	E_A	+	~2.01	200	All	1.4–1.3	—	2.0043 2.012	200 G at 300 μ s
5	E_B	+	2.0078	19	B	1.3	—	+ exch. 2.0043 2.012 + exch.	50 G at 300 ms 19 G at 300 μ s 50 G at 300 ms

A. Comparison with other data

Several ODMR studies in *a*-Si:H have been reported since 1978. It should be noticed first that the data we have described in the preceding section are different from those given by other authors. For example, we find one quenching and three enhancing signals while some others find two quenching and one enhancing,¹⁵ or two quenching and one enhancing signals.⁴ In order to clarify this situation, we have summarized the most important characteristics reported in the literature for the different lines. This summary is shown in Table II using the same format as for Table I. Note that the linewidths reported by the Xerox group cannot be directly compared to the others because these authors use a magnetic-field modula-

tion technique which yields derivative spectra.

We think, in agreement with other authors^{14,15} that the signal deconvolution made by the Japanese group can be questioned. The quenching lines (D_1, D_2) which they report can be attributed to an interference between one quenching and one enhancing lines. This type of overlap between lines results in the kind of signal of Fig. 2(b). This effect might also possibly be the cause of the observation by the Xerox group of two distinct quenching signals in their low-defect-density samples.¹⁵ So this overlap between signals might explain some of the discrepancies between the reports of these three groups and with ours. In any case, as we have seen in the preceding section, ODMR results are very sensitive to sample preparation and since each group has used different samples, a definite

TABLE II. Summary of the data in the literature.

Group	Name	Sign	<i>g</i> factor	Width (G)	Samples	Spectral dependence (eV)	Excitation dependence	Deconvolution	Time resolved
XEROX ^a	Q_1	—	2.0052	9 ^{pp}	B	1.4–1.3	0	2.0055	10 μ s–10 ms
	Q_2	—	2.0045	7	B low N_S	1.4	+	2.012 2.0043	1 μ s–10 μ s
$T=15$ K	E_1	+	2.0085	17	B low N_S	1.4	—	2.012 2.0043 + exch.	10 μ s–1 ms
HULL ^b	Q	—	2.005	14 ^{$H_{1/2}$}	All	1.45	—	2.0043 2.012	300 μ s→3 ms
	E	+	2.0065	16	stronger in A	0.9	+	2.0055 2.012	
$T=2$ K	E_1	+	2.008	20	B	1.25	—	2.0055	5 μ s–300 μ s
	E_2	+	2	200	All	1.25	—		
TOKYO ^c	D_1	—	2.018	~15 ^{$H_{1/2}$}	B	1.45		2.012	10 μ s–100 μ s
	D_2	—	2.006	~10	B	1.42		2.0055	
$T=2$ K	A_1	+	2	230	B	1.31		+ 2.0043	
	A_2	+	2.012	40	B	1.31			

^aReference 15.^bReferences 14, 17, and 20.^cReferences 4 and 36.

systematization of the results seems difficult to achieve. However, our results and classification of signals are usually in general agreement with those reported by the Hull group.¹⁴

B. The models of the literature

Two major recombination models have been suggested in order to explain these results: A distant-pair^{4,14} and a geminate model.^{15,24}

1. The distant-pair model

The distant-pair model was first suggested to explain donor-acceptor luminescence in crystalline semiconductors.²⁷ Although donor-acceptor luminescence does not occur in intrinsic *a*-Si:H, the distant-pair model is useful because it applies to any recombination involving pairs of independently-localized centers. When pairs consist of close centers, the exchange interaction between electron and hole is strong and the system must be considered as a bound exciton. When pairs are distant enough, exchange effects are negligible and the ODMR signals are characteristic of the radiative centers involved. At low temperature and at low-optical-excitation density, pairs are well defined. As required by the optical selection rules, the decay times (τ_p) of a pair which has two spins parallel is longer than the one (τ_{ap}) of the same pair when two spins are antiparallel. When the diffusion length of the photoexcited carriers during thermalization is larger than the mean-pair separation, the carriers' creation is of the distant-pair type²⁸ and pairs of both spin configurations are created in equal density. Now if the spin thermalization time T_1 is longer than the decay times, the density of antiparallel spin pairs rapidly becomes smaller than the density of parallel spin pairs. When microwave power is applied to the sample at the resonance conditions of either of the radiative centers, these two densities become equal, and so increases the density of the antiparallel spin pairs which enhances the luminescence intensity. Thus, the ODMR line is usually the superposition of the resonances of the two centers which form the radiative pairs. If the spin-dependent pair process shunts the luminescence mechanism being monitored, the sign of the ODMR signal is negative.

We have reported elsewhere computations of the recombination kinetics for this model.²⁵ These calculations yield theoretical responses of the PL intensity to square-wave modulation of the microwave power which agree with those reported by other authors.^{16,27} These theoretical responses are shown for spin-dependent radiative recombination of unthermalized carriers [Fig. 14(a)] (Ref. 27) and for a spin-dependent shunt process [Fig. 14(b), Ref. 16]. When the spin thermalization time is shorter than the radiative times the size of the ODMR effect is drastically decreased but the shape of the response remains almost unchanged.

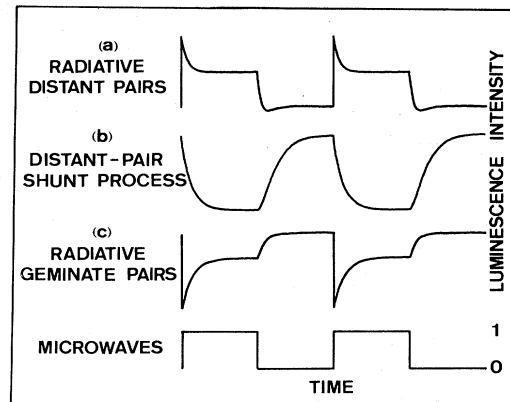


FIG. 14. Theoretical simulation of the response of the luminescence intensity to a square-wave modulation of the microwave power. The calculations used here have already been reported in Refs. 16 and 25.

2. The geminate model

This model was first suggested for chalcogenide glasses. It applies to systems where the diffusion length of the photoexcited carriers during thermalization is small. A photoexcited electron will then recombine with the hole with which it was created: This is geminate recombination. The optical selection rules are expected to yield geminate pair creation in the antiparallel spin configuration. If during thermalization in the bands and in the band tails, the carriers keep their spin memory, the pair will remain in the antiparallel spin configuration. The geminate model does not require any shunt process to explain enhancing and quenching signals.¹⁵

If the spin thermalization time T_1 is longer than the radiative lifetime, microwave power at resonance will equalize the parallel and antiparallel pair densities, will thus decrease the antiparallel pair density, and so quench the luminescence. The theoretical response to microwave modulation for this case is shown in Fig. 14(c).

If the time T_1 is shorter than the lifetime, the populations of the system's electronic levels follow more or less Boltzmann statistics and microwave power at resonance may create a small positive effect. The theoretical microwave response is similar to the one shown in Fig. 14(a).

C. The enhancing signal at $g=2.0065$

Comparison between the transient response to microwave modulation of this signal [Fig. 5(b)] and the theoretical curves of Fig. 14 clearly associates this signal with distant-pair radiative recombination. The positive spike measured at microwave switch on is typical of this kind of recombination mechanism. The spectral dependence of this line links it to the low-energy (0.9-eV) luminescence band (Fig. 4).

The deconvolution of this line into the dangling-bond resonance at $g=2.0055$ and the hole LESR resonance at $g=2.012$ [Fig. 3(b)], shows that this distant-pair radiative

recombination occurs between carriers localized at a silicon dangling bond and at a LESR hole center.

The LESR centers have been identified as band tail states.¹² This seems to be confirmed by thermostimulated ESR,²⁹ thermostimulated currents, and capacitance experiments.³⁰ Although this identification is still not definite, we will accept it here for the sake of simplicity. We have computed elsewhere⁷ the energy distribution of localized carriers in band tail states after photoexcitation at low temperature and we have suggested a model which we outlined in the Introduction and in which radiative states are band tail states' local minima. The slope of the exponential tails is derived from absorption and photoluminescence temperature dependence.^{7,31} The LESR hole state, i.e., a valence-band tail state, is neutral (V_t^0), diamagnetic, and has two valence electrons at equilibrium. It becomes positively charged (V_t^+), paramagnetic ($S = \frac{1}{2}$), when it loses one electron by localization of a photoexcited hole.

The dangling bond has three charge configurations: T_3^+ positively charged, diamagnetic, and has no valence electron; T_3^0 is neutral, paramagnetic ($S = \frac{1}{2}$), and one has one valence electron; T_3^- is negatively charged, diamagnetic, and has two valence electrons.¹²

Now, a spin-dependent effect happens only when both recombination centers are paramagnetic in the charge configuration at which recombination occurs. The enhancing signal at $g=2.0065$ is thus due to distant-pair radiative recombination between the valence electron of a dangling bond in the charge configuration T_3^0 and a hole localized at a valence-band tail state. Radiative recombination from a diamagnetic, negatively charged dangling bond T_3^- is also possible but cannot give any ODMR signal. This conclusion disagrees with a recently suggested model for the low-energy luminescence band³² where the T_3^0 states are not expected to be radiative.

The transient response of this signal to square-wave-chopped microwaves [Fig. 5(b)], and the low quantum efficiency of this low-energy luminescence band imply that this radiative process is shunted by a spin-independent, nonradiative mechanism, such as direct capture by the dangling bond of a hole in a delocalized state of the valence band.³³ If we assume that radiative recombination from a T_3^0 state is not Stokes shifted³² and since the spectral dependence of the ODMR signal on this radiative recombination culminates around 0.85 eV, the T_3^0 dangling-bond states would be located 0.85 eV above the valence-band's radiative tail states. We have drawn in Fig. 15, the density-of-states diagram in agreement with this conclusion. Since dangling bonds are paramagnetic when neutral and since they give an ESR signal in the dark, they must have a positive correlation energy U larger than the width of their distribution in energy.^{12,25} The energy level of the T_3^- is shifted by U on the energy scale from the T_3^0 state. In the diagram of Fig. 15, the location of the T_3^- state 0.6 eV below the conduction-band mobility edge fits with the extrinsic optical absorption spectrum peaking at 1.3 eV, Ref. 34, if absorption arises from optical transitions between electrons in delocalized states at the valence-band mobility edge and dangling

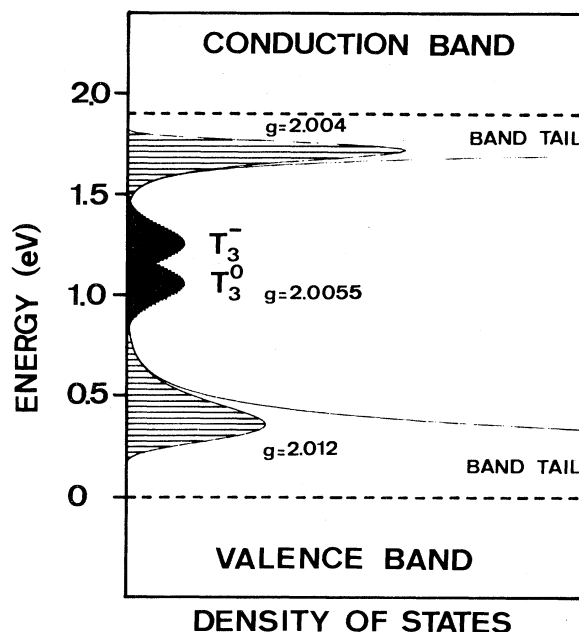


FIG. 15. Suggested density-of-states diagram for a -Si:H. Densities of states associated with dangling bonds and densities of band tail radiative states (as computed in Ref. 7) are both shown.

bonds ($h\nu = E_{T_3^-} - 0 = 1.3$ eV) rather than between dangling bonds and delocalized states at the conduction-band mobility edge ($h\nu = E_g - E_{T_3^0} = 1.9 - 1.1 = 0.8$ eV).

In this model the T_3^0 state is radiative at low energy. The low-energy luminescence band is stronger in p -type doped than in n -type doped samples.³² In p -type samples all dangling bonds are T_3^+ at equilibrium. As seen by LESR, under optical excitation, photoexcited electrons are captured by these dangling bonds which become T_3^0 . Strong 0.9-eV luminescence in these samples confirms that T_3^0 is radiative. On the other hand, we think that in n -type samples, all dangling bonds being in their T_3^- charge state, they capture photoexcited holes directly and nonradiatively. In this case direct capture is stronger than radiative tunneling because of the large-hole-capture cross section due to the negative charge of the T_3^- dangling bond.

D. The quenching signal at $g=2.005$

This signal was originally proposed as the first evidence for geminate recombination.²⁴ However, comparison between the transient response to microwave modulation of this signal [Fig. 5(a)] and the theoretical curves of Fig. 14 clearly associates this signal with distant-pair shunt processes.¹⁶ The spectral dependence of this line shows that these shunt processes pass the high-energy luminescence transition (Fig. 4).

These processes are either radiative or nonradiative. Since we have shown that the main luminescence band at

1.4 eV and the dangling-bond-associated luminescence band at 0.9 eV are the only radiative transitions in α -Si:H, these shunt processes cannot give rise to a PL band peaking below 0.75 eV as previously suggested.¹⁴ These shunt processes are either radiative at 0.9 eV or nonradiative.

The deconvolution of the quenching line at 2.005 into the three ESR and LESR resonances suggests that the valence- and the conduction-band tail states and the dangling bonds are involved in these shunt processes [Fig. 3(a)]. This deconvolution assigns a larger intensity to the dangling-bond resonance at $g=2.0055$. We think that two distinct mechanisms shunt the main luminescence transition: The first one, which we will call *A*, is partially radiative at 0.9 eV and involves a dangling bond and a hole in a valence-band tail state; the second one, called *B*, occurs through nonradiative recombination between a localized electron in the conduction-band tail and a dangling bond.

1. Process A

We have shown in the preceding paragraph that the enhancing signal at $g=2.0065$ involves both the dangling-bond and the valence-band tail states. Thus we suggest that the first quenching process associated with the 1.4-eV PL band (*A*) and the enhancing mechanism on the 0.9-eV band are in fact the same. We think that this process is a two-step mechanism.

Step 1 is radiative tunneling of the lone valence electron of a T_3^0 dangling bond toward a hole in a valence-band tail state. This step is rather slow, i.e., it occurs on a timescale similar to the luminescence decay. It may be bypassed by a fast, spin-independent, nonradiative capture of a delocalized hole.

Step 2 is a fast, spin-independent, nonradiative capture of an electron from a delocalized state of the conduction band by this now positively charged dangling bond. Non-radiative tunneling of an electron in a conduction-band tail state toward this dangling bond is also possible. However, we think that direct capture may dominate because of the large-electron-capture cross section of the positive dangling bond. The order in which these two steps happen is inverted when dangling bonds which are positively charged at equilibrium are involved.

Process *A* bypasses the main luminescence transition. The radiative mechanism in step 1 is the dominant process at low optical excitation density and since it is slow, it controls process *A*. As required by experiment, resonance of either the dangling bond at $g=2.0055$ or the valence-band tail state at $g=2.012$ will enhance process *A* and will then quench the 1.4-eV band. A schematic representation of this suggested process is displayed on Fig. 16(a).

2. Process B

The second shunt process we suggest is also a two-step mechanism. The first step is a nonradiative spin-dependent tunneling of an electron in a conduction-band tail state to a dangling bond in the T_3^0 neutral paramagnetic charge configuration. The tunneling rate is separation dependent and may be slow. At high-excitation density, this step may be bypassed by a direct spin-independent nonradiative capture of an electron in a delocalized state of the conduction band.

The second step is either nonradiative tunneling of this electron from the T_3^- dangling bond to a hole in a valence-band tail state or direct nonradiative capture of a

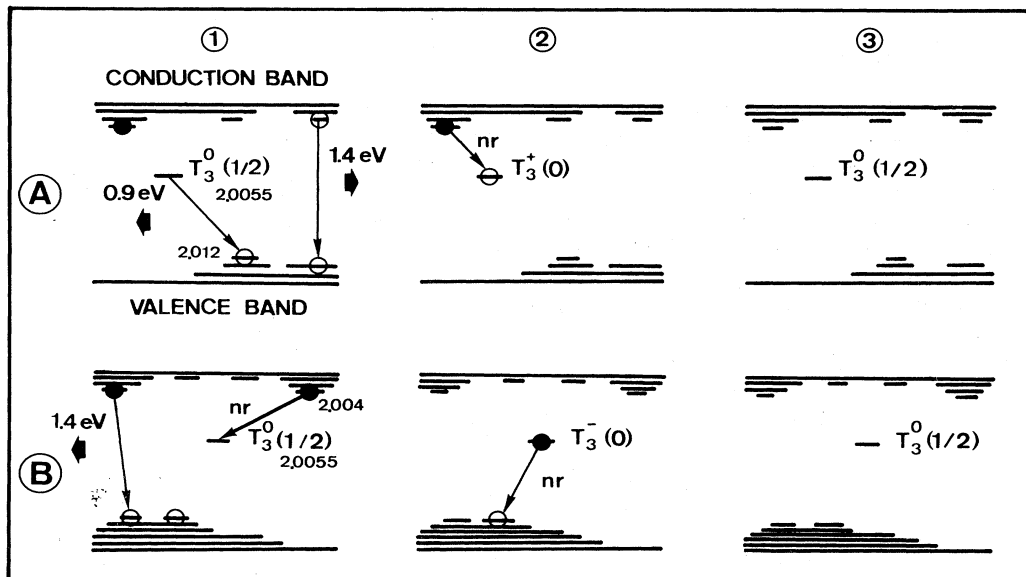


FIG. 16. Schematic representation of processes *A* and *B* suggested to explain the quenching ODMR signal at $g=2.005$. The arrows represent radiative transitions while nr stands for nonradiative. The spin of the dangling bond at the different stages of the processes is also shown.

hole in a delocalized state of the valence band by the negative T_3^- dangling bond. We think that under cw experiments, the latter dominates because of the large-hole-capture cross section of the negative dangling bond. Since T_3^- is diamagnetic this step is not spin dependent. The spin-dependent step 1 being slower than step 2 controls process *B*. Process *B* is nonradiative, spin dependent, and shunts the main luminescence transition. The ODMR line associated with it is the sum of the dangling-bond and the conduction-band tail state resonances at $g=2.0055$ and $g=2.004$, respectively. The different steps involved in process *B* are shown on Fig. 16(b).

Both spin-dependent quenching processes (*A* and *B*) shunt the 1.4-eV luminescence band and the combination of both effects on the luminescence intensity, yields the quenching ODMR line at $g=2.005$. At high optical excitation density, both spin-dependent quenching processes are bypassed by direct nonradiative spin-independent capture of delocalized carriers by dangling bonds. Thus the relative size of the quenching signal decreases at high-excitation density, in agreement with experiment.

This quenching signal is observed in our samples for temperatures less than 150 K, but observation at 300 K have been reported.⁴⁰ Room-temperature spin-dependent photoconductivity experiments display a very similar quenching signal.³⁵ So even in low-defect-density samples, in which radiative mechanisms dominate band-to-band recombination at low temperature, since 300-K luminescence efficiency is low (10^{-3}) the shunt processes associated with the quenching signal control room-temperature band-to-band recombination. Since in the recombination model described previously, we have related these recombination processes to dangling bonds, we conclude that the lifetime of the carriers at room temperature is controlled by the density and by the charge state of these defects.

E. The enhancing signals on the high-energy band

The similarity between the spectral dependence of these signals and the high-energy luminescence spectrum (Fig. 4) clearly associates the enhancing signals at $g \simeq 2.01$ and $g=2.0078$ with this band.

Although the response of these signals to microwave square-wave modulation [Fig. 5(c)] is of the form of the theoretical curves computed for radiative distant pairs [Fig. 14(a)], this experiment does not rule out the geminate model. If the spin of either of the carriers which form the pair thermalizes before recombination, both geminate and distant pairs yield the response of Fig. 14(a). However, the size of the effect should be much smaller than the one experimentally measured (0.5%) and we thus think that at low temperature pairs are unthermalized. The measurement of a TRODMR effect for delays longer than several seconds implies that the spin thermalization time T_1 of both recombination centers involved in the high-energy band is longer than one second. If the geminate carriers keep their spin memory, unthermalized geminate pairs give a quenching ODMR signal whose microwave transient response is similar to the one drawn on

Fig. 14(c). That is to say that all geminate pairs must be created and remain in the antiparallel spin configuration. Otherwise, if spin flips occur during thermalization of the photoexcited carriers in the bands and in the band tails, geminate and distant pairs are identical as far as spins are concerned. So ODMR cannot distinguish distant pairs from geminate pairs which have lost their spin memory. However, studies of the kinetics of the main luminescence band using frequency resolved spectroscopy^{25,18} have shown that recombination is distant pair in the range of optical excitation density used here.

We thus think that these enhancing signals arise from radiative (1.3–1.4 eV) recombination of unthermalized distant pairs. In the recombination model outlined in the Introduction, the high-energy luminescence arises from radiative recombination between carriers localized in band-tail-states' minima. Since the LESR centers have been identified as band tail states,¹² the ODMR and TRODMR signals on the high-energy band should thus be the superposition of the two LESR resonances at $g=2.004$ and $g=2.012$. However, this is not the case in any of the samples used.

This discrepancy and the difference between the cw spectral dependences of the enhancing and quenching signals led the Hull group to split the high-energy band into two components: The first band peaks at 1.25 eV, involves a radiative dangling bond, and gives the narrow enhancing ODMR signal measured in type-*B* samples¹⁷; the discrepancy between the g factor of the enhancing signal (2.0085) and the g factor of the dangling-bond resonance (2.0055) being explained by the interference of this signal with the quenching signal which is always present during cw experiments. The second PL band peaks at 1.4 eV, does not yield any enhancing signal but is by-passed by a spin-dependent mechanism which gives the quenching signal at $g=2.005$. However, no time-resolved ODMR data were available when this model was suggested and the effects of overlaps between signals have been minimized for spectral dependences and overestimated for g values. Since our pulsed-microwave TRODMR technique can isolate the different signals, definite g values and spectral dependences can be measured. We think that the radiative dangling-bond model is no longer feasible because of the difference between the narrow enhancing signal's measured g value of 2.0078 and the dangling-bond g value at 2.0055. Also, the identity between the time-resolved spectral dependences of the narrow enhancing signal and the quenching signal is in contradiction with the deconvolution of the high-energy luminescence spectrum into two bands.

We think instead, in agreement with other authors² that the main luminescence band arises from radiative recombination between carriers localized in band tail states^{25,7} and that the resonance lines of these radiative states differ from the LESR signals because of some nuclear or electronic interaction. The identification of an interaction which explains the different ODMR and TRODMR enhancing lines on the high-energy band, using only the two LESR resonances, is crucial for the feasibility of this model.

In type-*A* samples, the TRODMR signal for short delays is a 200-G-wide Lorentzian line. Such a large linewidth is quite a rare phenomenon in *X*-band spectroscopy. We will thus review and discuss all the interactions which may cause a 200-G-wide Lorentzian line.

Power broadening has been suggested as an explanation for this 200-G linewidth.¹⁵ However, although this broadening process may apply to ODMR results in type-*B* samples where the narrow signal and the broad line are superimposed and in which the latter may appear as wings of the former, it cannot apply to spectra measured in type-*A* samples where the broad line is isolated.

Homogeneous broadening yields a Lorentzian line shape which is in agreement with experiment but requires relaxation times as short as 10^{-10} s for a 200-G broadening. Such small values of T_1 and T_2 are not feasible. In any case, the intensity of an homogeneously broadened line is independent of field-modulation enhancement. Since this is in contradiction with experiment, homogeneous broadening cannot be responsible for the 200-G linewidth.

Anisotropy and distribution of the g tensor may broaden resonance lines. However, since g values must vary over more than 10% around the free-electron g value at 2.0023 in order to explain a 200-G linewidth in the *X* band, and since g factors are very close to 2.0023 in silicon because spin-orbit coupling is weak, this broadening effect is not feasible in *a*-Si:H.

Hyperfine interactions have been suggested³⁶ as a possible explanation of the 200-G linewidth. Hyperfine interaction is due to dipolar and contact interactions between nuclear and electronic spins. When this interaction takes place with a nucleus of spin I , an ESR or ODMR signal is split into $2 \times I + 1$ equal lines. If the hyperfine interaction is much weaker than the Zeeman interaction, the separation between these lines equals the size of this interaction. An ESR resonance is thus broadened when the size of the interaction is distributed. Since the nuclear spin of Si₂₈ is zero and the natural abundance of the next common silicon isotope (Si₂₉) which has a nuclear spin ($\frac{1}{2}$), is low (4.7%), it seems impossible²⁵ that a 200-G-wide Lorentzian line arises from hyperfine interaction with silicon nuclei. Protons have a nuclear spin ($\frac{1}{2}$). *a*-Si:H samples may contain up to 30% hydrogen and the ODMR 200-G-wide ODMR line is stronger in type-*A* samples (30%) than in type-*B* samples which contain less hydrogen (a few percent). However, if the 200-G linewidth is due to hyperfine interaction with protons, substitution of hydrogen by deuterium should decrease this linewidth by roughly the ratio of the gyromagnetic moments ($\gamma_H/\gamma_D=6.5$) of these isotopes. Since a 200-G line is still observed in *a*-Si:D samples (Fig. 12), we conclude that hyperfine interaction with protons is not the origin of this 200-G linewidth. However, our TRODENDOR experiments (Fig. 9) show that there are some weak dipolar hyperfine interactions between distant protons and the radiative states in *a*-Si:H.

The electron-hole exchange interaction arises from a purely quantum phenomenon and is indirectly linked to spins but may be represented by an isotropic spin opera-

tor,

$$\hat{H}_{ex} = J \hat{S}_e \cdot \hat{S}_h,$$

where ex denotes exchange. The size (J) of this interaction is proportional to the overlap integral of the wave function of both carriers³⁷ and is given by

$$J = J_0 \exp(-2r/r_0).$$

r_0 is the Bohr radius of the wave function of the less localized carrier. r is the separation between interacting carriers. J_0 should be similar to the size of the exchange interaction in a bound exciton in crystalline silicon: 2.10^5 G.³⁸ The smaller the pair separation, the stronger is the exchange interaction. The spin Hamiltonian associated with an electron-hole pair with exchange and in a magnetic field is given by

$$\hat{H}_s = \beta g_e \vec{H} \cdot \hat{S}_e + \beta g_h \vec{H} \cdot \hat{S}_h + \hat{H}_{ex}. \quad (1)$$

Diagonalization of this Hamiltonian yields the following eigenvalues and eigenstates³⁹:

$$|1\rangle = |+, +\rangle,$$

$$|2\rangle = |-, -\rangle,$$

$$|3\rangle = \cos\theta |+, -\rangle + \sin\theta |-, +\rangle,$$

$$|4\rangle = -\sin\theta |+, -\rangle + \cos\theta |-, +\rangle,$$

$$\theta = \frac{1}{2} \arctan \left[\frac{J}{\delta g \beta H} \right],$$

$$E_1 = \bar{g} \beta H + J/4,$$

$$E_2 = -\bar{g} \beta H + J/4,$$

$$E_3 = -J/4 + \left[\left(\frac{\delta g \beta H}{2} \right)^2 + \frac{J^2}{4} \right]^{1/2},$$

$$E_4 = -J/4 - \left[\left(\frac{\delta g \beta H}{2} \right)^2 + \frac{J^2}{4} \right]^{1/2},$$

$$\bar{g} = (g_e + g_h)/2,$$

$$\delta g = |g_e - g_h|.$$

$|+, +\rangle, |-, -\rangle, |+, -\rangle,$ and $|-, +\rangle$ are products of eigenstates of $\hat{S}_e^2, \hat{S}_{ez}, \hat{S}_h^2,$ and \hat{S}_{hz} . ODMR resonances occur at $H_0 \pm J/2\bar{g}\beta$ for the $1 \rightarrow 4$ ($-$) and $2 \rightarrow 4$ ($+$) transitions and at $H_0 \pm (\delta g/2)^2 (\beta H_0^2/J\bar{g})$ for the $1 \rightarrow 3$ and $2 \rightarrow 3$ transitions. The variations of the field position of these four resonances with increasing exchange interaction is shown in Fig. 17(a). Spin transition rates ($P_{ij} = |\langle i | g_e \hat{S}_{ex} + g_h \hat{S}_{hx} | j \rangle|^2$) between these eigenstates and the spin-dependent part of the radiative recombination rates ($R = |\langle i | f \rangle|^2$) from these eigenstates to the final state [$|f\rangle = (1/\sqrt{2}) |+, -\rangle - (1/\sqrt{2}) |-, +\rangle$] have also been computed and are displayed in Figs. 17(b) and 17(c), respectively.

Thus the two-line ODMR spectrum associated with a pair without exchange is changed to a four-line spectrum when exchange is present. From and between the two ini-

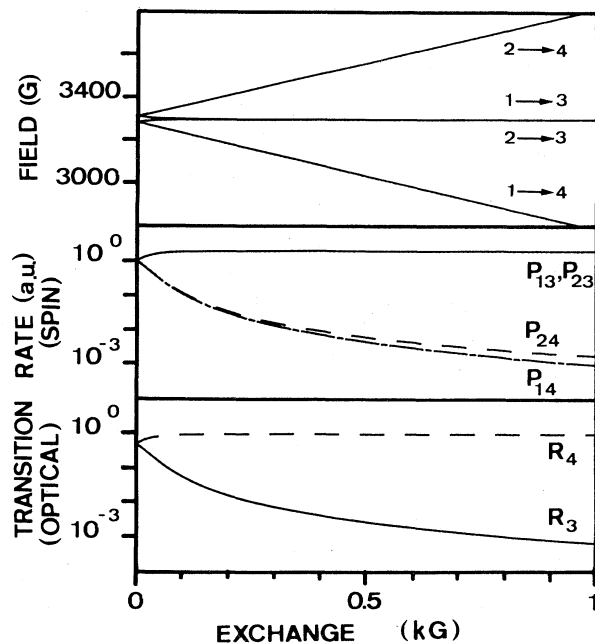


FIG. 17. Effect of exchange interactions on the field position of the resonances, on the spin transition rates, and on the optical transition rates (see text).

tial lines, two lines ($1 \rightarrow 3$ and $2 \rightarrow 3$) associated to allowed spin transitions ($P_{13} \simeq P_{23} \simeq 1$) move toward each other and merge into a single line at \bar{g} for infinite exchange. On each side of the initial ODMR spectrum an extra line ($1 \rightarrow 4$ or $2 \rightarrow 4$) moves away, becoming progressively forbidden as exchange is increased [Figs. 17(a) and 17(b)]. Since exchange interaction is a function of carrier separation and since we know from PL kinetics studies^{3,18} that this separation has a broad distribution, the size of the interaction, and consequently the field values for ODMR transitions, also have a wide distribution.

Depending on the relative size of the allowed and of the "forbidden" lines, the two initial resonances, i.e., the LESR spectrum ($J=0$) is either broadened (type-*A* samples) or replaced by a single line at the mean g value (type-*B* samples). The mean value of the conduction- and the valence-band tail states resonances seen in LESR, equals $(2.004 + 2.012)/2 = 2.008$ and is very close to the experimentally measured g factor in type-*B* samples. Increasing microwave power will enhance the forbidden spin transitions. This is in agreement with experiment since power-dependent wings have been reported in these samples¹⁵ and since the amplitude of the broad line is strongly power dependent in type-*A* samples.

Exchange interaction is often the origin of Lorentzian line shapes of resonance lines.³⁹ This is in agreement with the experimentally measured Lorentzian profiles of the enhancing lines at $g \simeq 2.01$ and $g = 2.0075$.

But most of all, exchange interactions are quite successful in explaining our TRODMR results. The radiative

recombination rate between two localized carriers is also proportional to the overlap integral of the wave function of both carriers³:

$$\tau = \tau_0 \exp(2r/r_0).$$

τ_0 should be similar to the lifetime of a bound exciton in crystalline silicon $\simeq 10^{-8}$ s.³⁸

Thus since TRODMR selects pairs of given separation, it measures ODMR effects for a given exchange interaction. However, since disorder distributes the ratio τ_0^{-1}/J_0 and since decay times are selected at best within a decade, a single exchange value cannot be isolated, and resolved lines cannot be observed. Nevertheless, the mean value of J is shifted toward strong exchange for short delay times and toward weak exchange for long delay times. In type-*A* samples, where the spectrum arises from forbidden spin transitions, strong exchange should broaden the line at short delay times and this line should narrow as the mean value of the exchange interaction is decreased at longer delay times. In type-*B* samples, where allowed transitions dominate, strong exchange should narrow the line at short delays and this line should broaden at longer times. Both effects agree with experiment (Figs. 8 and 13). Even for the longest delay times where TRODMR spectra have been measured (300 ms), these spectra still differ from the LESR signal. Since LESR strongly favors long-lived carriers (lifetime larger than seconds) (Ref. 28) we think that this discrepancy shows that even for 300-ms delays TRODMR spectra are still subject to exchange broadening.

The difference between the two types of samples still remains to be explained. A tentative explanation is the following: We suggest that an increase of the hyperfine interaction with protons from type-*B* samples (a few percent of H) to type-*A* samples (30% H) can explain the differences between the two kinds of samples. In type-*B* samples, the spin Hamiltonian given by Eq. (1) is a good enough approximation. The ODMR signal associated with the allowed transitions can be observed, since radiative rates from states $|1\rangle$, $|2\rangle$ ($R_1 = R_2 = 0$), and $|3\rangle$ ($R_3 > 0$) are different and carriers accumulate in states $|1\rangle$ and $|2\rangle$. On the other hand, in type-*A* samples, in order to take into account hyperfine interaction of electrons and holes with protons, two terms must be added to the main Hamiltonian. States $|1\rangle$ and $|2\rangle$ are then linear combinations of $|++\rangle$, $|--\rangle$, $|+-\rangle$, and $| - + \rangle$ and become radiative ($R_1, R_2 > 0$). Since R_3 decreases when exchange is increased [Fig. 17(c)], R_1 , R_2 , and R_3 could become similar and the ODMR signal associated with allowed spin transitions vanishes.

This explanation is also consistent with the TRODMR signal in *a*-Si:D which we have reported in this paper (Fig. 12). This spectrum is a compromise between the one measured in type-*A* samples and the one from type-*B* samples under the same experimental conditions. Although the deuterium concentration should be similar to the hydrogen concentration in type-*A* samples, hyperfine interactions are decreased by roughly the ratio of the gyromagnetic moments ($\simeq 6.5$) of these isotopes. States $|1\rangle$ and

$|2\rangle$ are thus less radiative and a superposition of the allowed and of the forbidden spin transitions is observed.

We think that exchange interactions have no noticeable effects on the quenching signal because this signal arises mainly from nonradiative tunneling transitions. Rates (τ_{nr}^{-1}) for such transitions are also given by

$$\tau_{nr} = \tau_{nr0} \exp(2r/r_0),$$

and $\tau_{nr0} \simeq 10^{-12}$ s (Ref. 15). Since $\tau_0 \simeq 10^{-8}$ s for radiative transitions, and since $J = J_0 \exp(-2r/r_0)$, exchange will be 4 orders of magnitude weaker for nonradiative pairs than for radiative pairs of similar lifetime.

We conclude that exchange interaction explains successfully the characteristics of the ODMR and TRODMR enhancing lines on the high-energy PL band, using only the two components of the LESR signal. We thus think that this study supports a model in which the high-energy PL band in *a*-Si:H arises from radiative recombination between weakly localized carriers in the band tail states.⁷ However, since a spectrum identical to the LESR spectrum is not observed by an ODMR technique, a model in which the high-energy PL band does not arise from the LESR centers cannot be completely ruled out.

V. CONCLUSION

In this paper we have reported the spin dependence of recombination in *a*-Si:H. Among the different techniques used, our pulsed-microwave time-resolved experiments proved to be the most precise and the most reliable method since interferences between signals of similar *g* factor can be minimized. Also, this technique revealed large time-dependent effects on linewidth.

We find four distinct spin-dependent processes; however, two of them arise from the same mechanism and are treated together.

(i) A quenching line on the high-energy PL band at $g=2.005$ arises from mainly nonradiative spin-dependent shunt processes and involves silicon dangling bonds.

(ii) An enhancing line on the low-energy PL band at

$g=2.0065$ results from distant-pair, spin-dependent, radiative recombination between a dangling bond and a hole localized in a band tail state. This recombination participates in the processes which shunt the high-energy luminescence band.

(iii a) A 200-G-wide enhancing line at $g \simeq 2.01$ on the high-energy PL band is measured in low-defect-density sputtered samples and arises from radiative recombination of carriers localized in band tail states. The initial band-tail state resonances as observed by LESR are broadened in ODMR through forbidden spin transitions by exchange interactions.

(iii b) A narrow enhancing line at $g=2.0078$ on the high-energy PL band is measured in all other samples and results also from the same spin-dependent radiative recombination mechanism as in (iii a). However, the initial band-tail state resonances merge into a single line due to allowed spin transitions resulting also from exchange interactions.

Both of the latter lines [(iii a) and (iii b)] arise from a single recombination process and we suggest that the choice between the two (allowed or forbidden) is controlled through hyperfine interaction by the hydrogen concentration in the sample.

We thus think that ODMR and TRODMR data is consistent with and generally supports the recombination model which we have previously suggested for the high-energy photoluminescence band in *a*-Si:H.⁷ Dangling bonds are also shown to be responsible for the 0.9-eV PL band and to be involved in nonradiative recombination, too.

ACKNOWLEDGMENTS

I wish to thank Professor I. Solomon, Dr. J. Magariño, and Mr. R. Cuchet for providing samples, Dr. E. Ligeon for the hydrogen concentration measurements, Mr. R. Picard for skilled technical assistance, Dr. D. J. Dunstan, Dr. S. P. Depinna, Dr. R. T. Cox, Dr. J. J. Davies, Dr. A. Hervé, and Dr. D. Kaplan for helpful discussions.

*Present address: Laboratoire Central de Recherches, Thomson-CSF, Boite Postale 10, F-91401 Orsay, France.

¹D. Engemann and R. Fischer, in *Amorphous and Liquid Semiconductors*, edited by J. Stuke and W. Brenig (Taylor and Francis, London, 1973), p. 947.

²R. A. Street, *Adv. Phys.* **30**, 593 (1981).

³C. Tsang and R. A. Street, *Phys. Rev. B* **19**, 3027 (1979).

⁴K. Morigaki, D. J. Dunstan, B. C. Cavenett, P. Dawson, J. E. Nicholls, S. Nitta, and K. Shimakawa, *Solid State Commun.* **26**, 981 (1978).

⁵R. A. Street, *Philos. Mag. B* **37**, 35 (1978).

⁶D. J. Dunstan and F. Boulitrop, *J. Phys. (Paris) Colloq.* **42**, C4-331 (1981).

⁷F. Boulitrop and D. J. Dunstan, *Phys. Rev. B* **28**, 5923 (1983).

⁸G. K. Walters and T. L. Estle, *J. Appl. Phys.* **32**, 1854 (1961).

⁹A. Friederich and D. Kaplan, *J. Electron. Mater.* **8**, 80 (1979).

¹⁰J. C. Knights, D. K. Biegelsen, and I. Solomon, *Solid State Commun.* **22**, 133 (1977).

¹¹R. A. Street, J. C. Knights, and D. K. Biegelsen, *Phys. Rev. B* **18**, 1880 (1978).

¹²R. A. Street and D. K. Biegelsen, *J. Non-Cryst. Solids* **35** and **36**, 651 (1980).

¹³D. Block and R. T. Cox, *J. Lumin.* **24** and **25**, 167 (1981).

¹⁴S. Depinna, B. C. Cavenett, I. G. Austin, T. M. Searle, M. J. Thomson, J. Allison, and P. G. Lecomber, *Philos. Mag. B* **46**, 473 (1982).

¹⁵R. A. Street, *Phys. Rev. B* **26**, 3588 (1982).

¹⁶S. Depinna, B. C. Cavenett, T. M. Searle, and I. G. Austin, *Philos. Mag. B* **46**, 501 (1982).

¹⁷S. Depinna, B. C. Cavenett, I. G. Austin, and T. M. Searle, *Solid State Commun.* **41**, 263 (1982).

¹⁸D. J. Dunstan, S. P. Depinna and B. C. Cavenett, *J. Phys. C*

- 15, L425 (1982).
- ¹⁹D. Block, A. Hervé, and R. Cox, *Phys. Rev. B* **25**, 6049 (1982).
- ²⁰S. P. Depinna and B. C. Cavenett, *J. Phys. C* **15**, L489 (1982).
- ²¹D. Kaplan, I. Solomon, and N. F. Mott, *J. Phys.* **39**, 1 (1978).
- ²²R. T. Cox and F. Boulitrop (unpublished).
- ²³J. J. Davies, *J. Phys. C* **11**, 1907 (1982).
- ²⁴D. K. Biegelsen, J. C. Knights, R. A. Street, C. Tsang, and R. M. White, *Philos. Mag. B* **37**, 477 (1978).
- ²⁵F. Boulitrop, thesis, Université Scientifique et Médicale de Grenoble, 1982 (unpublished).
- ²⁶R. A. Street, D. K. Biegelsen, and J. C. Knights, *Phys. Rev. B* **24**, 969 (1981).
- ²⁷D. J. Dunstan and J. J. Davies, *J. Phys. C* **12**, 2927 (1979).
- ²⁸F. Boulitrop and D. J. Dunstan, *Solid State Commun.* **44**, 841 (1982).
- ²⁹J. Dijon, F. Boulitrop, and D. J. Dunstan (unpublished).
- ³⁰J. Dijon, *Solid State Commun.* (in press).
- ³¹F. Boulitrop, D. J. Dunstan, and A. Chenevas-Paule, *Phys. Rev. B* **25**, 7860 (1982).
- ³²R. A. Street, *Phys. Rev. B* **21**, 5775 (1980).
- ³³D. J. Dunstan, *Phys. Rev. B* **28**, 2252 (1983).
- ³⁴W. B. Jackson and N. M. Amer, *Phys. Rev. B* **25**, 5559 (1982).
- ³⁵I. Solomon, D. K. Biegelsen, and J. C. Knights, *Solid State Commun.* **22**, 505 (1977).
- ³⁶K. Morigaki, P. Dawson, B. C. Cavenett, D. J. Dunstan, S. Nitta, and K. Shimakawa, in *Proceedings of the 14th Conference on Amorphous and Liquid Semiconductors, Edinburgh, 1978*, edited by B. C. H. Wilson (Institute of Physics, Bristol, 1979), p. 1163.
- ³⁷P. W. Anderson, *Solid State Phys.* **14**, 99 (1963).
- ³⁸M. L. W. Thewalt, *Can. J. Phys.* **55**, 1463 (1977).
- ³⁹A. Abragam and B. Bleaney, *Electron Paramagnetic Resonance Of Transition Ions* (Clarendon, Oxford, 1970).
- ⁴⁰S. Depinna, B. C. Cavenett, T. M. Searle, and I. G. Austin, *Solid State Commun.* **43**, 79 (1982).